IEEE Access
Multidisciplinary ⋮ Rapid Review ⋮ Open Access Journal

Received 31 August 2023, accepted 30 September 2023, date of publication 9 October 2023, date of current version 13 October 2023.

Digital Object Identifier 10.1109/ACCESS.2023.3322973

RESEARCH ARTICLE

Two-Dimensional Inclinometer/Tilt Sensor With a Large Dynamic Range Utilizing Half-Wavelength Microstrip Resonator

SHABNAM AHMADI ANDEVARI[1], JOSE-LUIS OLVERA-CERVANTES[2], AND CARLOS E. SAAVEDRA[1]

[1]Department of Electrical and Computer Engineering, Queen's University, Kingston, ON K7L 3N6, Canada
[2]Instituto Nacional de Astrofisica, Optica y Electronica (INAOE), Puebla 72840, Mexico

Corresponding author: Shabnam Ahmadi Andevari (19saa6@queensu.ca)

This work was supported in part by the Natural Sciences and Engineering Research Council of Canada (NSERC) under Grant RGPIN-2022-05204.

ABSTRACT This article presents a 2-D inclinometer consisting of two individual sensors oriented orthogonally to one another such that each sensor measures the tilt angle along its respective axis. The sensors are constructed using a combination of a half-wavelength microstrip transmission line on a printed circuit board and a rotating transmission line on an overlapping circuit board. As the inclination angle changes, the overall length of the resonator varies, leading to a shift in the resonance wavelength. This wavelength shift accurately represents the inclination variation. The experimental results demonstrate a sensitivity of 0.507 mm/° and a resolution of 0.029° for the sensor. The inclinometer offers a wide dynamic tilt angle measurement range of at least 80° (±40°) along any axis in XY plane. Additionally, the proposed inclinometer exhibits simplicity, cost-effectiveness, and robustness.

INDEX TERMS Inclinometer, microstrip, microwave, resonator, sensor, tilt, dynamic range, resolution, sensitivity, 3D printing, two-dimensional.

I. INTRODUCTION

Inclinometers measure the angular deviation of a surface or system from a reference plane, indicating the degree of inclination. In recent times, the demand for inclination sensors has significantly increased across a wide range of applications, including construction, mining, geotechnical and geological monitoring, navigation systems, robotics, and industrial automation [1], [2], [3], [4], [5]. Currently, there is a wide range of commercial inclinometers available for these applications. However, the growing demand for improved inclinometers in terms of performance, cost, and durability has driven continuous research in this field [5], [6].

Over the past few years, there have been numerous reports and advancements in the field of electromagnetic and optical inclinometers [1], [2], [3], [4], [5], [6], [7], [8], [9], [10], [11], [12]. However, the majority of these inclinometers are limited to measuring the inclination along a single known axis, and the sensor needs to be properly aligned with this axis. To address this limitation, two-dimensional (2-D) inclinometers have been developed. These specialized devices are capable of simultaneously measuring inclination angles along two orthogonal directions, even when inclination along a random axis in the XY plane is applied. This makes them highly versatile in scenarios where the inclination axis is unknown. A common approach for 2-D inclination measurements involves combining two or more inclinometers, enabling independent measurement of inclination along the orthogonal X and Y directions [13], [14], [15].

In [15], a temperature-insensitive 2-D inclinometer was proposed by combining two fiber Bragg gratings (FBGs) attached to a deliberately designed pendulum. The pendulum, which was composed of a tapered cylindrical beam and a mass, served as the foundation for accurate inclination measurements. FBG-based inclinometers operate on the principle

The associate editor coordinating the review of this manuscript and approving it for publication was Ali Karami Horestani.

that a change in tilt angle leads to a modification in the strain applied to the FBGs. Consequently, this strain alteration results in a shift of the resonance wavelength. In [16], a different implementation of a 2-D inclinometer using FBGs is presented. This particular inclinometer involves the crisscross arrangement of two etched chirped fiber Bragg gratings (CFBG) arrays, with each array consisting of two symmetrically arranged CFBGs. Reference [14] introduces another variant of an optical 2-D inclinometer. This inclinometer design incorporates a pair of Extrinsic Fabry-Perot Interferometers (EFPI) that are arranged in a perpendicular configuration. EFPI inclinometers are primarily constructed with two parallel reflective surfaces positioned with a gap in between, which functions as the sensing element. When the inclinometer is tilted, this gap undergoes variations in response. Fiber-optic inclinometers are known for their high accuracy, sensitivity, and minimal transmission loss. However, they may not always be suitable for applications in harsh environments that demand robust construction and durability. Additionally, the associated interrogation system for fiber-optic inclinometers can be costly [3], [15], [17].

Considering their superior durability when compared to optical fibers, coaxial cables offer a promising solution for implementing inclinometers. In [18], a 2-D coaxial cable inclinometers, which is inspired by optic-fiber EFPIs, is examined. In contrast to its optic-fiber counterparts, this inclinometer provides both robustness and high resolution capabilities. Nevertheless, a drawback of this inclinometer is its bulkiness and limited angle measurements range. Other variations of electromagnetic-based inclinometers include capacitive inclinometers [19] and microstrip resonator-based inclinometers [1], [20]. However, to date, there have been no attempts to implement a 2-D inclinometer using these particular methods.

In this article, a cost-effective and robust two-dimensional (2-D) inclinometer is introduced. This inclinometer offers a wide angle measurement range, along with relatively high sensitivity and resolution. It is also more compact and lightweight compared to the previously discussed 2-D inclinometers that utilized optical or coaxial cable technology. The design of the proposed 2-D inclinometer is inspired by the inclinometer sensor presented in [1]. The proposed approach incorporates two angular half-wavelength microstrip resonators (HWMRs), each comprising a fixed component and a movable component that overlaps with it. These two sensors are strategically positioned perpendicular to each other, facilitating precise measurement of tilt angles in two dimensions.

The paper is structured as follows: It begins by exploring the resonator design method, followed by discussions on the 2-D inclination sensing arrangements and the corresponding required Physical configuration. The experimental results obtained from the inclinometer are then presented and thoroughly analyzed. A comprehensive discussion and comparison with other inclinometers are carried out to assess the performance of the proposed approach.

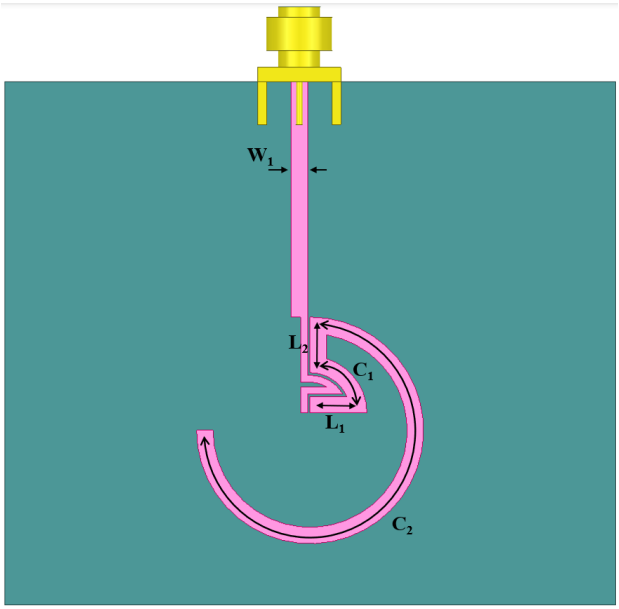

FIGURE 1. The layout of the angular half-wavelength resonator; C1 is a 90° circular sector line and C2 is a θ° circular sector line.

II. INCLINOMETER DESIGN PRINCIPLE

A. INCLINATION SENSING WITH RESONANCE SYSTEM

Half-wavelength resonators have found application in various microwave sensors [1], [21], [22]. The resonator depicted in Fig. 1 is the foundation of the sensor proposed in this work. It is designed as an open-ended half-wavelength microstrip line, arranged in a circular path. A coupling structure is designed to measure the resonant frequency of the resonator at the input port. The shape and dimensions of the coupling structure are chosen such that a strong coupling as well as a high quality-factor is maintained. The substrate selected for the resonator is RO4003C, with a dielectric constant (ε_r) of 3.38±0.05, a loss tangent of 0.0027, a copper cladding thickness (t) of 34 um, and a dielectric thickness (h) of 0.81 mm. Considering C1 as a 180° section of a circle with a radius of L1 and C2 as a θ° section of a larger circle with a radius of L1 + L2, the resonance wavelength of the resonator is given as [1].

$$\lambda_n = \frac{2}{n}(L_1 + \frac{\pi}{2}L_1 + L_2 + \theta(L_1 + L_2)) \tag{1}$$

where θ is the section angle of the outer circular part of the resonator and c is the speed of light, and n is an integer representing the resonant mode. Due to the linear relationship between the resonance wavelength and the tilt angle, we have chosen to utilize the resonance wavelength as our sensing element.

In a similar manner to [1], a fixed part and a moving part that have an overlap constitute an overlapping structure, as shown in Fig. 2. However, the distinction in this case is that the section angle of the outer circular part of the fixed component and the section angle of the moving element are set at 180°. Consequently, when the inclination angle θ_i is 0°,

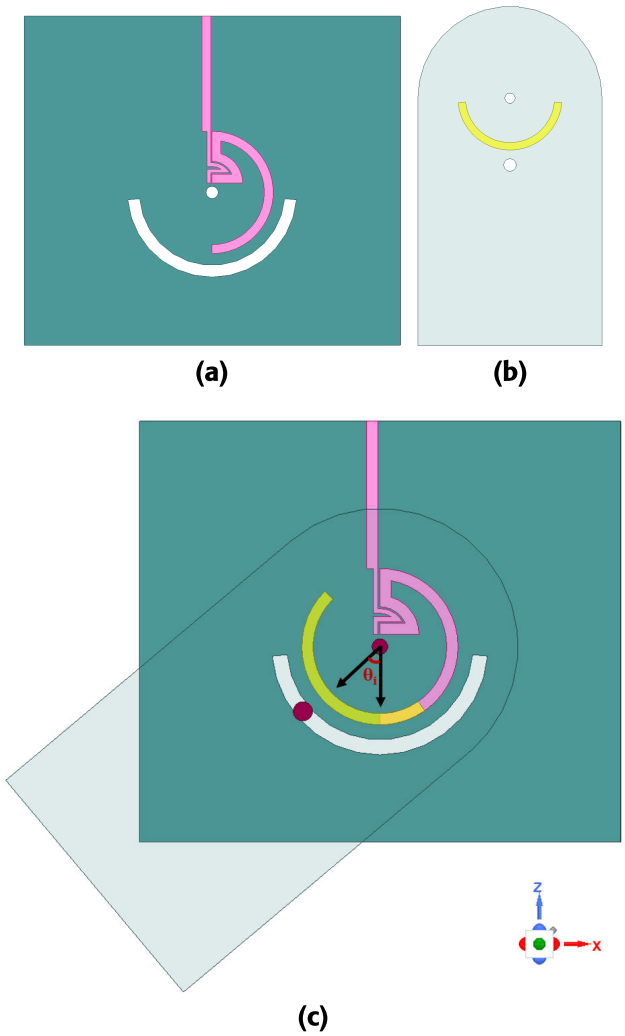

FIGURE 2. (a) Fixed part, (b) moving part, and (c) the overlapped schematic at a given inclination angle θ_i to the left ($\theta = 225° + \theta_i$); in case of inclination to the right, θ_i would be negative. The pink line shows the fixed part, the green line shows the moving part, and the yellow section indicates the overlapped area.

the resulting angle θ would be 270°. The magnitude of the reflection coefficients at the input port for the sensor inclined by different θ_i angles are shown in Fig. 3.

B. 2-D INCLINATION SENSING ARRANGEMENT

A one dimensional inclinometer measures the tilt angle along one axis but provides no information on the tilt of the plane on which the inclinometer sits. To address this issue, certain arrangements are made to enable 2-D inclination sensing.

When an inclination is applied along the X axis (the axis of sensor positioning) in [1], the moving part functions like a pendulum and moves in response to the force of gravity due to the relatively heavy weight connected to the sliding part through a string. When the inclination axis has a component in both the X and Y directions ($I = x\hat{i} + y\hat{j}$), the fixed and moving parts may become disconnected or the moving part may not move with gravity, depending on the sign of the

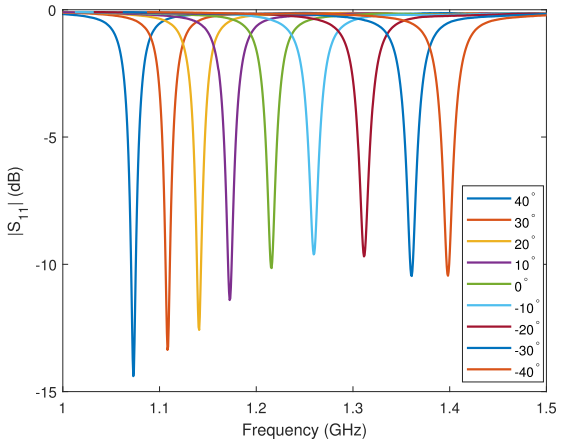

FIGURE 3. The magnitude of the measured reflection coefficient for the sensor at various inclination angles θ_i.

Y component. If the Y component of the inclination axis is positive, indicating that the sensor is bent towards the front, the weight force pulls the outer edge of the moving part away from the fixed part, resulting in a loss of connection between them. If the Y component is negative, indicating that the sensor is tilted backward, the weight will be stopped by the edge of the sensor, as the string will be held in place, preventing the moving part from moving.

When addressing the disconnection issue, the initial approach involved working with the airgap between the moving and fixed parts by developing a model to understand their coupling. The theoretical premise was that tilting the sensor along the X-axis by an angle θ_y in the forward Y-direction would lead to corresponding adjustments in the airgap between the two parts. This adjustment was expected to result in different θ_x vs. f_x relationships for varying θ_y angles while still exhibiting a logical trend. However, experimental testing revealed that the anticipated behavior did not manifest as expected.

The underlaying cause of this discrepancy was the inconsistent change in the airgap with respect to θ_y, influenced by external factors such as vibrations and variations in the tightness of screws, which significantly affected its behavior. Furthermore, the sensor's sensitivity to inclination decreased notably as the airgap increased, reaching a point where sensitivity became negligible, rendering the inclinometer unusable.

Consequently, to achieve a practical and effective 2-D inclinometer, we pursued an alternative approach to ensure that the two parts of the sensor are in direct electric contact. To prevent disconnection between the static and moving parts of the inclinometer, an extra securing point is introduced near the outer circular microstrip line, as illustrated in Fig. 4. Since the sliding part moves in a circular motion, a circular gap path is created on the fixed part to enable the moving part to move freely while still being firmly attached by a bolt that moves with it. Moreover, the shape of the moving part itself resembles that of a pendulum, and the weights are attached

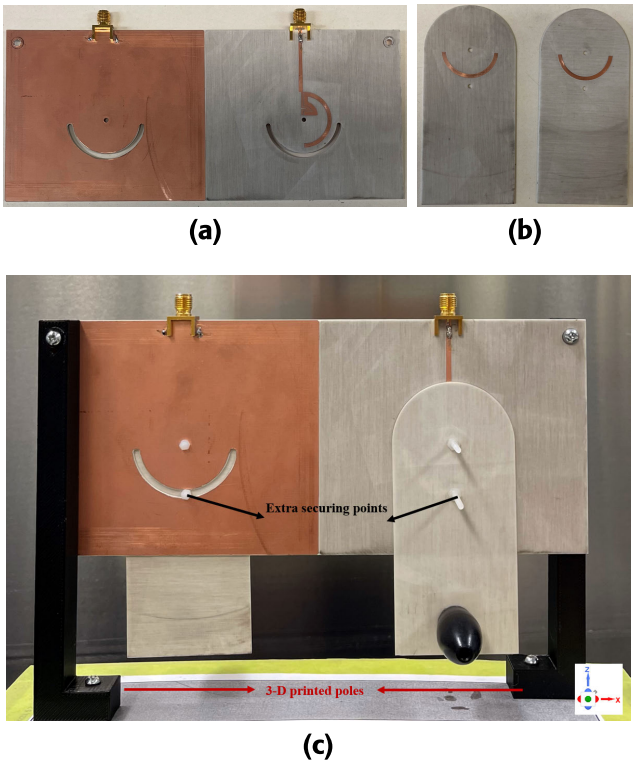

FIGURE 4. Fabricated inclinometer: (a) fixed part, (b) moving part, (c) overlapped structure.

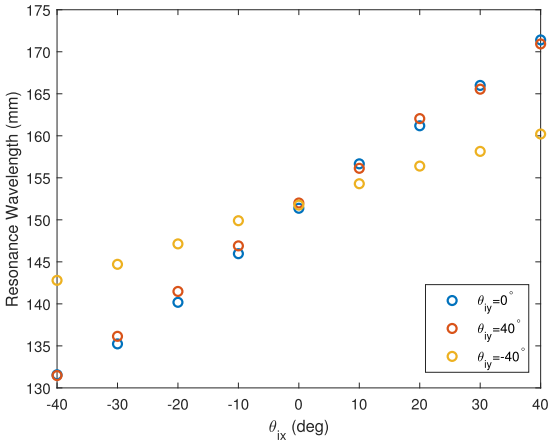

FIGURE 5. Resonance wavelength of the sensor as a function of θ_{ix}, when θ_{iy} is 0°, 40°, and −40°.

to it directly using an adhesive, rather than a string as in [1]. This configuration prevents hindrance of the weight's movement when tilting backward, a problem that can arise with a pendulum constructed using a string.

Figure 5 shows the resonance wavelength of the sensor in three different conditions as a function of inclination angle. The inclination angles along the X and Y axes are denoted by θ_{ix} and θ_{iy}, respectively. The sensor is inclined along the X axis from $-40°$ to $40°$ under three conditions: the first with θ_{iy}=0°, the second with θ_{iy}=40°, and the third with θ_{iy}=−40°. The first two graphs exhibit a similar trend, whereas the third one deviates from them. This result is observed when the sensor is tilted backward, where the weight force is not the only factor affecting the movement.

If θ_{iy} is zero, the weight force acts solely parallel to the surface of the sensor. Therefore, in this scenario, the pendulum equation can be written as $mgsin\theta_x = 0$, where m is the weight's mass, g is the is gravitational constant, and θ_x represents the angle between the pendulum axis and the direction of the gravitational force. As this angle is zero, the system behaves like a regular, balanced pendulum and the movement of the sliding part is correlated to the inclination angle.

When θ_{iy} is nonzero, the weight force has two components: $mgcos\theta_{iy}$ along the parallel direction, and $mgsin\theta_{iy}$ along the perpendicular direction. Tilting the sensor backward causes the perpendicular weight force to push the sliding part toward the fixed part, adding to the force generated by the screw tightening. As a result, this perpendicular force creates friction in the opposite direction of the sliding part's movement. The friction force, which is proportional to the parallel force ($f_s = \mu mgsin\theta_{iy}$, where μ is the coefficient of friction), affects the pendulum equation. It becomes $mgcos\theta_{iy}sin\theta_x - \mu mgsin\theta_{iy} = 0$, resulting in $\theta_x = sin^{-1}(\mu tan\theta_{iy})$. This means that there is a difference between the pendulum axis and the direction of the gravitational force, causing the sliding part to move less than the applied inclination. This is the reason why the yellow plot in Fig. 5 shows a smaller slope, indicating a lower sensitivity to inclination. To maintain a consistently high sensitivity across the entire dynamic inclination range, two identical sensors are fabricated on opposite sides of the substrate. Thus, when the front sensor is tilted backward, the back sensor is tilted forward and we only use the measurements taken from the forward tilted sensor each time. Thus, one sensor is used for $\theta_{iy} > 0$ and the other for $\theta_{iy} < 0$.

When the sensor is tilted forward, the force that pulls the moving part inward with the screw reacts to the weight force that pulls it outward, effectively canceling out the perpendicular component of the weight force. Consequently, this scenario can be considered similar to the case when θ_{iy} is zero, except for the fact that the parallel force decreases as θ_{iy} deviates further from zero. The sensor's dynamic inclination measurement range is restricted due to this. Bolts are tightened to the maximum extent that still allows the weight force to move the sliding part smoothly. However, as the weight force in parallel to the surface decreases, there will come a point where it will no longer be able to move the sliding part. In our experiments, the sliding part remained free to move with θ_{iy} up to 40°, indicating that the dynamic range of the 2-D inclination measurement range is at least ±40° based on experimental results. We were restricted to conducting experiments within a maximum range of approximately ±40°. The limitations of the commercial inclinometer prevented us from exploring a broader range of inclinations. The primary purpose of the

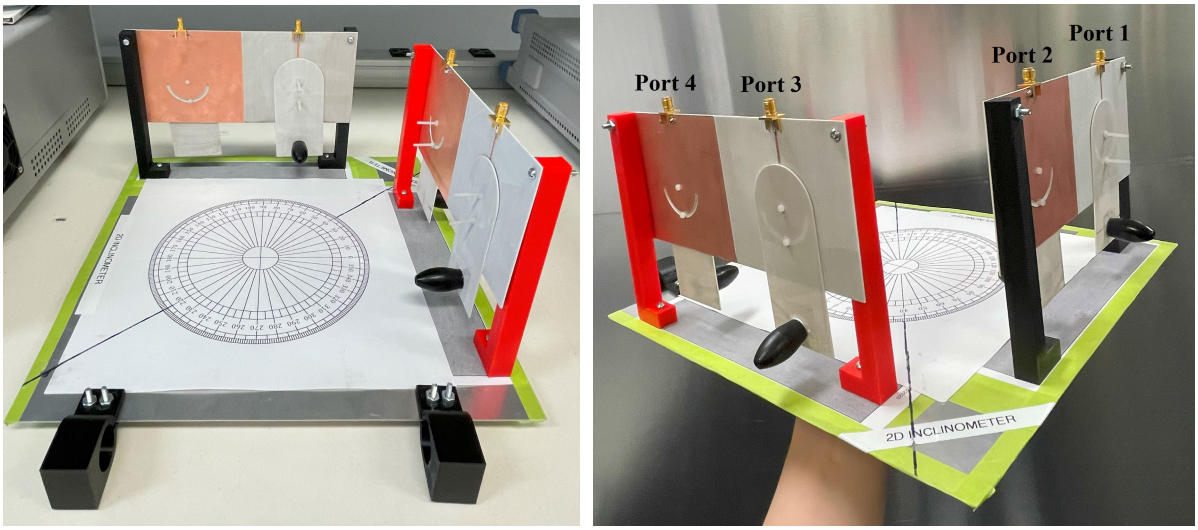

FIGURE 6. The mechanical configuration for the inclinometer setup: (a) front view, (b) side view.

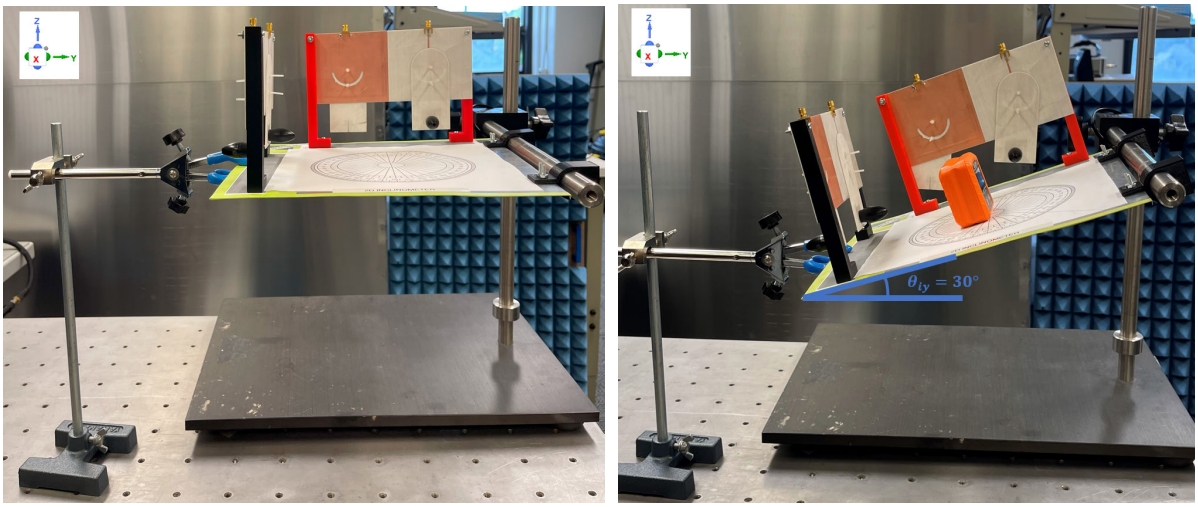

FIGURE 7. Inclination measurement setup: (a) zero inclination, (b) 30° inclination.

commercial inclinometer was to maintain a zero inclination along the perpendicular axis with respect to the inclination axis. However, when an inclination greater than 40° was applied, the inclinometer was unable to accurately measure the angle along the perpendicular axis and instead displayed an error comment. Hence, the actual dynamic range is likely to be larger, though we couldn't experimentally prove it. Additionally, increasing the dynamic range further is feasible by using a heavier weight in the setup. However, we are currently unable to demonstrate this due to the limitations of the commercial inclinometers, which we require as references for our measurements.

The proposed 2-D inclinometer consists of two sets of sensors positioned in two perpendicular axes, X and Y. The next section discusses the details of how the X and Y inclination angles can be determined using the four measurements taken from the four resonators.

C. PHYSICAL CONFIGURATION OF INCLINOMETER

For the physical configuration of the 2-D inclinometer, it is necessary to ensure the sensors are securely positioned vertically in relation to the inclination plane. Additionally, it is crucial to arrange the two sensors at a precise 90-degree angle to each other. The proposed setup is illustrated in Fig. 6. The physical setup involves utilizing two 3-D printed poles positioned at the edges of each sensor. These poles are attached to the sensors using bolts and then securely fastened to a flat surface at the bottom.

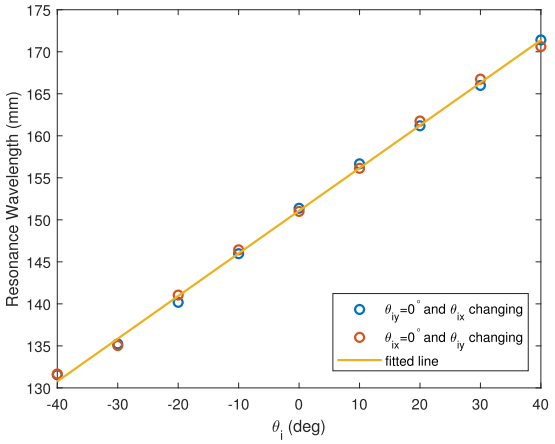

FIGURE 8. Resonance wavelength of the inclinometer as a function of applied inclination in large angle variation experiment.

To allow free rotation of the moving part without interference, the poles are designed to be sufficiently long. Moreover, they are strategically placed on opposite sides of the sensor to prevent any hindrance to the sliding part. This arrangement eliminates the need for a larger sensor size, as there is ample space for the moving part to maneuver before reaching the poles. As a result, the sensor size is minimized to its fullest extent.

III. EXPERIMENTAL RESULTS

A. INCLINATION ANGLE VARIATION TEST

The experimental arrangement for inclinometer measurement is depicted in Fig. 7. On one side, the inclinometer is supported by two clamps affixed to a beam of fixed height. On the opposite side, it is connected to a movable clamp positioned along a vertical axis on a pole. By adjusting the position of the second clamp on the pole, the sensor package can be inclined to varying angles. Depending on the intended inclination axis, the positions of the clamps on the sensors are adjusted accordingly. This alignment ensures that the clamps are aligned with the axis along which the inclination will be applied. To facilitate the alignment process, a protractor is placed on the flat surface that holds the sensors. This protractor serves as a reference tool for accurately controlling the inclination axis during the setup procedure.

In the experiment, a specific scenario with $\theta_{iy} = 0$ is conducted, and inclination angles (θ_{ix}) ranging from $-40°$ to $+40°$ with $10°$ increments along X axis are applied. For each angle setting where $\theta_{iy} < 0$, the reflection coefficient at the first port (S_{11}) is measured, and for settings where $\theta_{iy} > 0$, the reflection coefficient at the second port (S_{22}) is measured using a vector network analyzer (VNA). The resonance frequencies corresponding to each measurement are recorded. Fig. 8 illustrates the relationship between the resonance wavelength of the sensor and the inclination angle. As the applied inclination angle varies from $-40°$ to $+40°$, the resonance wavelength exhibits an increasing trend, consistent with the expectations derived from (1).

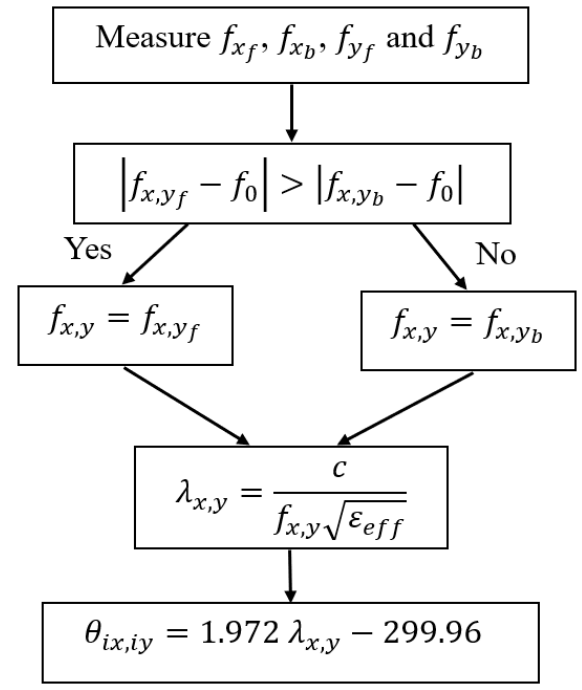

FIGURE 9. Flow diagram outlining the process of determining inclination angles.

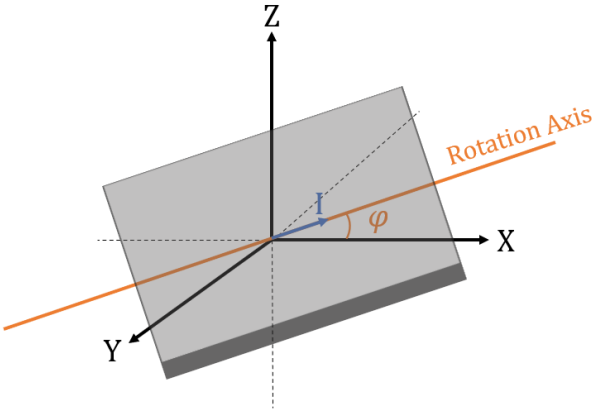

FIGURE 10. Random rotation axis in XY plane.

The measured data has been fitted to a linear curve, resulting in (2)

$$\lambda = 0.507\theta_i + 152.08 \tag{2}$$

where λ is measured in mm and θ_i in degrees. As a result, the measurement sensitivity is determined to be 0.507mm/°. A commercially available inclinometer has been employed to keep θ_{iy} fixed while varying θ_{ix}. The accuracy of the commercial inclinometer is approximately $\pm 1°$, which accounts for the minor deviations observed in the plot.

An additional experiment is conducted with a fixed X inclination angle of θ_{ix}=0, while the Y inclination angle (θ_{iy}) is varied from $-40°$ to $40°$. The measurements obtained from

TABLE 1. Random inclination axis test results.

φ	θ	f_{xf}	f_{yf}	Measured θ_{ix}	Measured θ_{iy}	Expected θ_{ix}	Expected θ_{iy}
50°	**19.6°**	1.151 GHz	1.163 GHz	15.27°	12.04°	14.98°	12.56°
40°	**-19.6°**	1.261 GHz	1.271 GHz	-12.34°	-14.44°	-12.56°	-14.98°
-30°	**30°**	1.271 GHz	1.114 GHz	-14.52°	25.7°	-14.88°	25.91°
-60°	**-30°**	1.321 GHz	1.273 GHz	-25.46°	-14.92°	-25.91°	-14.88°

TABLE 2. Performance comparison with recent inclinometers.

REF	Sensor Configuration	Axis	Dynamic Range	Sensitivity	Resolution
[4]	FBG	2-D	0° to 90°	9.22 pm/°	0.15°
[16]	FBG	2-D	0° to 2.5°	3.3 nm/°	0.003°
[14]	EFPI	2-D	-0.48° to 0.48°	1.05 mm/°	$5.7*10^{-7}$°
[18]	HCC-FPR	2-D	0° to 7.2°	350 MHz/°	$6.3*10^{-6}$°
THIS WORK	HWMR	2-D	-40° to 40°	0.507 mm/°	0.029°

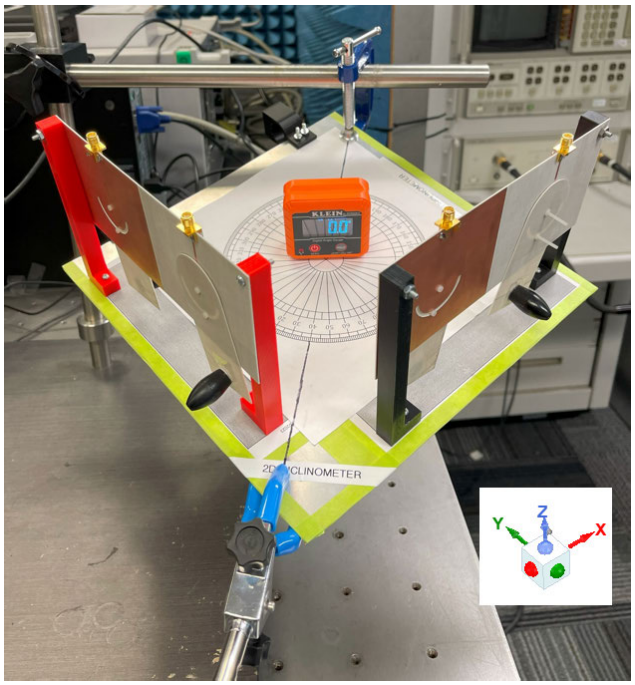

FIGURE 11. Applying inclination along a random axis in the XY plane.

ports 3 and 4, as shown in Fig. 8, are utilized to establish the resonance wavelength as a function of the Y inclination angle. Given the use of identical sensors in both experiments, the resulting functions are also identical. As a result, the curve expression obtained from the fitting process in (2) can be effectively used to represent the data obtained from the second perpendicular sensor as well.

Moreover, as illustrated in Fig. 5, altering the perpendicular inclination does not affect the data obtained from parallel inclination variations. Thus, the data presented in Fig. 8 remains reliable across all scenarios. To further validate this assertion, another test is conducted. In this test, θ_{ix} is fixed at 0 using the commercial inclinometer, while θ_{iy} is varied from $-40°$ to $40°$ in 10-degree increments. The resonance wavelength of the sensor along the X-axis is then measured at ports 1 and 2. The nine recorded wavelengths exhibit a maximum deviation of 0.68 mm, which can be attributed to the error associated with the commercial inclinometer. Considering the accuracy of the commercial inclinometer, θ_{ix} experiences a variation of approximately $\pm 1°$. It is worth noting that a 2-degree change in inclination corresponds to a 1.14 mm change in wavelength. Since the measured deviation is 0.68 mm, which is smaller than the expected change, it can be concluded that this deviation is mainly caused by the slight variations in θ_{ix}. Thus, as long as we have knowledge of the resonance wavelength at the four ports, we can accurately determine the inclination angles along the X and Y axes.

Finally, a resolution test similar to [1] was performed, involving slight variations in inclination angles. The test revealed a resolution of 0.029° for the 2-D inclinometer. Furthermore, the sensitivity for small-scale inclination variations was determined to be 0.504mm/°, which closely matches to the sensitivity observed during larger inclination variations.

B. PROCESS FOR DETERMINATION OF 2-D INCLINATION ANGLES

The process of determining the X and Y inclination angles is illustrated in the flow diagram shown in Fig. 9. The resonance

frequencies measured at ports 1 to 4 are denoted as f_{x_f}, f_{x_b}, f_{y_f} and f_{y_b}, respectively. As previously mentioned, we will utilize the measurements from the forward tilted sensor, which exhibits a greater deviation from the zero-inclination condition, as depicted in Fig. 5. The resonance frequency of the sensor at $\theta_{ix,iy}$=0 is represented as f_0 and has a value of 1.22 GHz. Therefore, among the frequencies f_{x,y_f} and f_{x,y_b}, the ones that differ more significantly from f_0 are selected for further analysis. Subsequently, the corresponding resonance wavelength is calculated, and finally, the inclination angles $\theta_{ix,iy}$ are determined using the last equation in the diagram, which is an alternative form of (2).

C. RANDOM INCLINATION AXIS TEST

First, our objective is to ascertain the degree of inclination for both the X and Y axes when the XY plane is tilted by an angle of $\theta°$ about the axis in the XY plane that forms an angle of $\varphi°$ with the X axis, as depicted in Fig. 10. The vector I represents the unit vector describing the axis of rotation and can be expressed as $I = cos\varphi\hat{i} - sin\varphi\hat{j}$. To determine the rotated unit vectors x' and y', corresponding to the original vectors $x = 1\hat{i}$ and $y = 1\hat{j}$, we can utilize the Rodrigues' rotation formula.

$$v' = vcos\theta + (I \times v)sin\varphi + I(I.v)(1 - cos\theta) \tag{3}$$

where the vectors v and v' can be substituted with x or y and x' or y', respectively. Thus, the vectors x' and y' can be determined using (4) and (5).

$$x' = (cos\theta + (1 - cos\theta)cos^2\varphi)\hat{i} + (cos\varphi sin\varphi(cos\theta - 1))\hat{j} + (sin\varphi sin\theta)\hat{k} \tag{4}$$

$$y' = (cos\varphi sin\varphi(cos\theta - 1))\hat{i} + (cos\theta + (1 - cos\theta)sin^2\varphi)\hat{j} + (cos\varphi sin\theta)\hat{k} \tag{5}$$

The angles θ_{ix} and θ_{iy}, which represent the inclination of the X and Y axes respectively, can be computed by determining the angles between the original vectors x and y, and their corresponding rotated vectors x' and y'. By applying the formula for the angle between two vectors, given as $\theta_{ab} = cos^{-1}\frac{a.b}{|a||b|}$, we can determine the values of θ_{ix} and θ_{iy} as (6) and (7), as shown at the top of the next page.

In this section, the system is subjected to inclinations around random axes with different φ values. The protractor is utilized to control the inclination axis, while the clamps are aligned with the line perpendicular to the inclination axis, as shown in Fig. 11. The commercial inclinometer is carefully aligned with the inclination axis to ensure that it displays a reading of zero degrees for the perpendicular angle. The test is conducted for four sets of φ and θ, and the corresponding resonance wavelengths of the front or back sensor are recorded. The recorded data is presented in Table 1. Using (2), the X and Y inclination angles are calculated, along with the expected θ_{ix} and θ_{iy} from (6) and (7), respectively. It is observed that there is a difference of less than 0.5 mm between the expected and measured θ_{ix} and θ_{iy} for all four cases. This discrepancy is primarily attributed to the experimental test equipment, specifically the reference commercial inclinometer, as discussed in the previous section.

IV. COMPARING RECENT 2-D INCLINOMETERS

Table 2 presents a comparison between the proposed 2-D inclinometer developed in this study and the inclinometers described in recent literature. The proposed sensor in this article offers the ability to measure inclination along two perpendicular axes, regardless of the orientation of the 2-D inclination axis. It can accurately measure inclination angles within the dynamic range of −40° to 40°, with a sensitivity and resolution of 0.507 mm/° and 0.029°, respectively.

The two-dimensional (2-D) FBG inclinometer presented in [4] offers a wide dynamic range but lacks high resolution. Conversely, the inclinometer discussed in [16] demonstrates relatively high resolution but is restricted in terms of its angle measurement dynamic range. When translating our sensor's sensitivity to frequency shift versus tilt angle, it yields an approximate average value of 5 MHz/°. In comparison, the sensor in [18] exhibits a higher sensitivity but is constrained to a small dynamic measuring range of only 7.2° for tilt angles. The 2-D inclinometers in [14] has also a restricted inclination measurement range despite having exceptionally high resolution. Notably, the proposed sensor in this paper offers a significantly wide dynamic range along with high resolution and sensitivity. It also provides the benefit of simplicity in comparison to other high-performance 2-D inclinometers described in the available literature. Additionally, it is durable, lightweight, relatively compact in size, and benefits from a cost-effective fabrication process and interrogation system.

V. CONCLUSION

The article introduces a 2-D inclinometer that utilizes two sensors positioned orthogonally. In a real-world application, the sensor would be encased in a shielded box to prevent radiation leakage and to protect the moving parts. Each sensor consists of two angular half-wavelength microstrip line resonators, one located at the front and the other at the back of the sensor. This configuration ensures a consistently high sensitivity throughout the entire dynamic range of inclination along any inclination axis. Each resonator comprises a fixed part and a sliding part, and as the inclinometer is tilted, these parts can overlap, resulting in a change in the resonator's length. These variations in length correspond to changes in the resonators' resonance wavelength, enabling the measurement of the inclination angle along two perpendicular axes.

The proposed inclinometer offers several advantages, including robustness, simplicity, and cost-effectiveness. It is capable of accurately detecting inclination angles along two axes with a high resolution and sensitivity. Moreover, it outperforms other inclinometers discussed in recent literature by providing a larger dynamic range.

$$\theta_{ix} = cos^{-1}\frac{cos\theta + (1-cos\theta)cos^2\varphi}{\sqrt{(cos\theta + (1-cos\theta)cos^2\varphi)^2 + (cos\varphi sin\varphi(cos\theta - 1))^2 + (sin\varphi sin\theta)^2}} \quad (6)$$

$$\theta_{iy} = cos^{-1}\frac{cos\theta + (1-cos\theta)sin^2\varphi}{\sqrt{(cos\varphi sin\varphi(cos\theta - 1))^2 + (cos\theta + (1-cos\theta)sin^2\varphi)^2 + (cos\varphi sin\theta)^2}} \quad (7)$$

REFERENCES

[1] S. A. Andevari, J. L. Olvera-Cervantes, and C. E. Saavedra, "Inclination sensor with a wide angle measurement range using half-wavelength microstrip resonator," *IEEE Access*, vol. 11, pp. 7358–7368, 2023.

[2] I. Matsuya and O. Furuya, "Design of optical inclinometer composed of a ball lens and viscosity fluid to improve focusing," in *Proc. IEEE SENSORS*, Oct. 2022, pp. 1–4.

[3] A. Gautam and A. Kumar, "Highly sensitive FBG based tilt sensor using PM-IM conversion and EFD interrogation technique," *IEEE Trans. Instrum. Meas.*, vol. 71, pp. 1–9, 2022.

[4] B. Yuan, Z. Zhao, and Y. Yuan, "Two-dimensional inclinometer based on an elastic cylinder cantilever and eight FBGs," *IEEE Sensors J.*, vol. 22, no. 3, pp. 2172–2181, Feb. 2022.

[5] Y. Xu, Q. Jiang, K. Yang, J. Zhou, and Q. Guo, "A novel ultra-high-resolution inclination sensor based on diamagnetic levitation," *Sens. Actuators A, Phys.*, vol. 343, Aug. 2022, Art. no. 113686.

[6] T. S. Sarkar, S. Das, B. Chakraborty, and H. S. Dutta, "Absolute encoder-based dual axis tilt sensor," *IEEE Sensors J.*, vol. 19, no. 7, pp. 2474–2481, Apr. 2019.

[7] Y. Yang, E. Wang, K. Chen, Z. Yu, and Q. Yu, "Fiber-optic Fabry–Pérot sensor for simultaneous measurement of tilt angle and vibration acceleration," *IEEE Sensors J.*, vol. 19, no. 6, pp. 2162–2169, Mar. 2019.

[8] J. Cui, D. S. Gunawardena, Z. Liu, Z. Zhao, and H.-Y. Tam, "All-fiber two-dimensional inclinometer based on Bragg gratings inscribed in a seven-core multi-core fiber," *J. Lightw. Technol.*, vol. 38, no. 8, pp. 2516–2522, Apr. 15, 2020.

[9] K. Kinjalk, A. Kumar, and A. Gautam, "High-resolution FBG-based inclination sensor using eigen decomposition of reflection spectrum," *IEEE Trans. Instrum. Meas.*, vol. 69, no. 11, pp. 9124–9131, Nov. 2020.

[10] M. Maheshwari, Y. Yang, D. Upadrashta, and T. Chaturvedi, "A rotation independent in-place inclinometer/tilt sensor based on fiber Bragg grating," *IEEE Trans. Instrum. Meas.*, vol. 68, no. 8, pp. 2943–2953, Aug. 2019.

[11] R. W. Mok, P. Silveira, A. Dante, C. Carvalho, M. Keley, L. Garção, R. Allil, and M. Werneck, "Inclination sensor based on FBG with enhanced sensitivity," in *Proc. IEEE Int. Instrum. Meas. Technol. Conf. (I2MTC)*, May 2018, pp. 1–5.

[12] S. Wang, Y. Yang, L. Mohanty, R.-B. Jin, and P. Lu, "Ultrasensitive fiber optic inclinometer based on dynamic Vernier effect using push–pull configuration," *IEEE Trans. Instrum. Meas.*, vol. 71, pp. 1–8, 2022.

[13] H. Y. Au, S. K. Khijwania, H. Y. Fu, W. H. Chung, and H. Y. Tam, "Temperature-insensitive fiber Bragg grating based tilt sensor with large dynamic range," *J. Lightw. Technol.*, vol. 29, no. 11, pp. 1714–1720, Jun. 2011.

[14] Y. Zhuang, Y. Chen, C. Zhu, R. E. Gerald, Y. Tang, and J. Huang, "A high-resolution 2-D fiber optic inclinometer for structural health monitoring applications," *IEEE Trans. Instrum. Meas.*, vol. 69, no. 9, pp. 6544–6555, Sep. 2020.

[15] H. Bao, X. Dong, L.-Y. Shao, C.-L. Zhao, C. C. Chan, and P. Shum, "Temperature-insensitive 2-D pendulum clinometer using two fiber Bragg gratings," *IEEE Photon. Technol. Lett.*, vol. 22, no. 12, pp. 863–865, Jun. 2010.

[16] H.-Y. Chang, Y.-C. Chang, and W.-F. Liu, "A highly sensitive two-dimensional inclinometer based on two etched chirped-fiber-grating arrays," *Sensors*, vol. 17, no. 12, p. 2922, Dec. 2017.

[17] J. Guo, C. Zhu, Y. Tang, and J. Huang, "Temperature-insensitive inclinometer based on transmission line Fabry–Pérot resonators," *IEEE Trans. Instrum. Meas.*, vol. 71, pp. 1–10, 2022.

[18] C. Zhu, Y. Tang, Y. Zhuang, J. Guo, R. E. Gerald, and J. Huang, "2-D tilt sensor based on coaxial cable Fabry–Pérot resonators with submicroradian resolution," *IEEE Trans. Microw. Theory Techn.*, vol. 70, no. 4, pp. 2398–2406, Apr. 2022.

[19] O. Ozioko, H. Nassar, and R. Dahiya, "3D printed interdigitated capacitor based tilt sensor," *IEEE Sensors J.*, vol. 21, no. 23, pp. 26252–26260, Dec. 2021.

[20] A. K. Horestani, Z. Shaterian, and M. Mrozowski, "A compact and lightweight microwave tilt sensor based on an SRR-loaded microstrip line," in *Proc. 24th Int. Microw. Radar Conf. (MIKON)*, Sep. 2022, pp. 1–3.

[21] S. A. Andevari, J.-L. Olvera-Cervantes, H.-N. Morales-Lovera, and C. E. Saavedra, "Dual-band uniaxial dielectric anisotropy sensor using coupled-line resonators," *IEEE Access*, vol. 11, pp. 7358–7368, 2023.

[22] L. Su, J. Muñoz-Enano, P. Vélez, P. Casacuberta, M. Gil, and F. Martín, "Phase-variation microwave sensor for permittivity measurements based on a high-impedance half-wavelength transmission line," *IEEE Sensors J.*, vol. 21, no. 9, pp. 10647–10656, May 2021.

SHABNAM AHMADI ANDEVARI received the B.Sc. degree in electrical engineering from the Babol Noshirvani University of Technology, Babol, Iran, in 2014, the M.Sc. degree in electrical engineering from the Amirkabir University of Technology, Tehran, Iran, in 2017, and the Ph.D. degree in electrical engineering from Queen's University, Kingston, ON, Canada, in 2023. Her research interests include microwave sensors, material characterization, mechanical motion detection, and RF circuit design.

JOSE-LUIS OLVERA-CERVANTES received the B.Sc. degree from Instituto Politécnico Nacional, Mexico City, Mexico, in 2001, and the M.Sc. and Ph.D. degrees from Centro de Investigación Científica y de Educación Superior de Ensenada, Ensenada, Mexico, in 2005 and 2008, respectively. In 2009, he joined Instituto Nacional de Astrofísica, Óptica y Electrónica, where he is currently a Full Professor. His research interests include microwave sensors, radar systems, dielectric characterization, food properties, and signal processing.

CARLOS E. SAAVEDRA received the Ph.D. degree in electrical engineering from Cornell University, Ithaca, NY, USA. He is currently a Professor and the Head of the Department of Electrical and Computer Engineering, Queen's University, Kingston, ON, Canada. He is a licensed Professional Engineer (P.Eng.) in the Province of Ontario. He is the former Co-Chair of the NSERC Discovery Grants Evaluation Group 1510 and he has served on grant review panels with the U.S. National Science Foundation. He is a former Associate Editor of IEEE TRANSACTIONS ON MICROWAVE THEORY AND TECHNIQUES, a Guest Editor of IEEE OPEN JOURNAL OF ANTENNAS AND PROPAGATION, and a Guest Editor of the *IEEE Microwave Magazine*.